

ARTICLE

Received 23 Jul 2012 | Accepted 8 Mar 2013 | Published 16 Apr 2013

DOI: 10.1038/ncomms2720

OPEN

Molecular mechanics of mineralized collagen fibrils in bone

Arun K. Nair¹, Alfonso Gautieri^{1,2}, Shu-Wei Chang¹ & Markus J. Buehler^{1,3,4}

Bone is a natural composite of collagen protein and the mineral hydroxyapatite. The structure of bone is known to be important to its load-bearing characteristics, but relatively little is known about this structure or the mechanism that govern deformation at the molecular scale. Here we perform full-atomistic calculations of the three-dimensional molecular structure of a mineralized collagen protein matrix to try to better understand its mechanical characteristics under tensile loading at various mineral densities. We find that as the mineral density increases, the tensile modulus of the network increases monotonically and well beyond that of pure collagen fibrils. Our results suggest that the mineral crystals within this network bears up to four times the stress of the collagen fibrils, whereas the collagen is predominantly responsible for the material's deformation response. These findings reveal the mechanism by which bone is able to achieve superior energy dissipation and fracture resistance characteristics beyond its individual constituents.

¹Laboratory for Atomistic and Molecular Mechanics (LAMM), Department of Civil and Environmental Engineering, Massachusetts Institute of Technology, 77 Massachusetts Avenue, Room 1-235 A and B, Cambridge, Massachusetts 02139, USA. ²Biomechanics Group, Department of Electronics, Information and Bioengineering, Politecnico di Milano, Via Golgi 39, 20133 Milan, Italy. ³Center for Computational Engineering, Massachusetts Institute of Technology, 77 Massachusetts Avenue, Cambridge, Massachusetts 02139, USA. ⁴Center for Materials Science and Engineering, Massachusetts Institute of Technology, 77 Massachusetts Avenue, Cambridge, Massachusetts 02139, USA. Correspondence and requests for materials should be addressed to M.J.B (email: mbuehler@MIT.EDU).

Bone is a remarkable hierarchical biomaterial (Fig. 1a) that has two major constituents, soft collagen protein and much stiffer apatite mineral^{1,2}. During the formation of bone, collagen molecules assemble into fibrils, which are mineralized via the formation of apatite crystals. Although larger-scale bone structures differentiate depending on bone type and species, the structure of mineralized fibrils is highly conserved across species and different types of bone, and hence act as the bone's universal elementary building block^{3–6}. The hierarchical structure of bone enables it to be a light-weight material that can carry large loads, and combines the toughness of inorganic material and the flexibility of protein-based tissues^{7–12}. Previous studies based on mechanical models have uncovered key mechanistic features of bone as well, eluded to the role of mineral platelets in strengthening the material^{13–18}. At the nanoscale, the interactions between collagen molecules and the mineral hydroxyapatite (HAP), and as well as the amount of mineral, are known to have a significant role in providing strength and toughness to the bone (or lack thereof, in disease states). In this paper we focus on the structure and mechanics of mineralized collagen fibrils, as it is universally found in many types of bone. Collagen–HAP composites are not only the basic building blocks of the human bone, but they are also amongst the most abundant class of biomineralized materials in the animal kingdom (found in the skeletal system, teeth or antler)^{1,2}.

Although the structure of bone and its mechanical properties have been well-studied, the knowledge about how collagen fibrils and HAP crystals interact at the molecular scale, and how they deform as an integrated system under external stress are not well understood. Developing a deeper understanding of the properties of bone from the level of its building blocks requires a thorough investigation of the interplay of the organic protein molecules with the mineral crystals. This, in turn, requires an atomistic-level investigation of the properties of the organic–inorganic interfaces^{19,20} and its correlation with the overall mechanical behaviour. Several attempts have been made to develop a molecular model of bone, but those studies fell short to providing a full three-dimensional, chemically and structurally accurate model of the interactions of collagen with the mineral phase^{21–24}. Coarse-grain models²⁵ of nascent bone showed that the mineral crystals provide additional strength and also increases the Young's modulus and fracture strength. Although these models provided some insight into the mechanics of bone, they failed to capture atomic-scale mechanisms, did not reach higher mineralization levels, and did not allow for a direct comparison with experimental work (for example, *in situ* x-ray analysis of bone deformation^{1–6}). The coarse-grain description of nascent bone²⁵ is a highly simplified two-dimensional model and relies on empirically derived mechanical parameters, which were not directly derived from fundamental principles of chemical

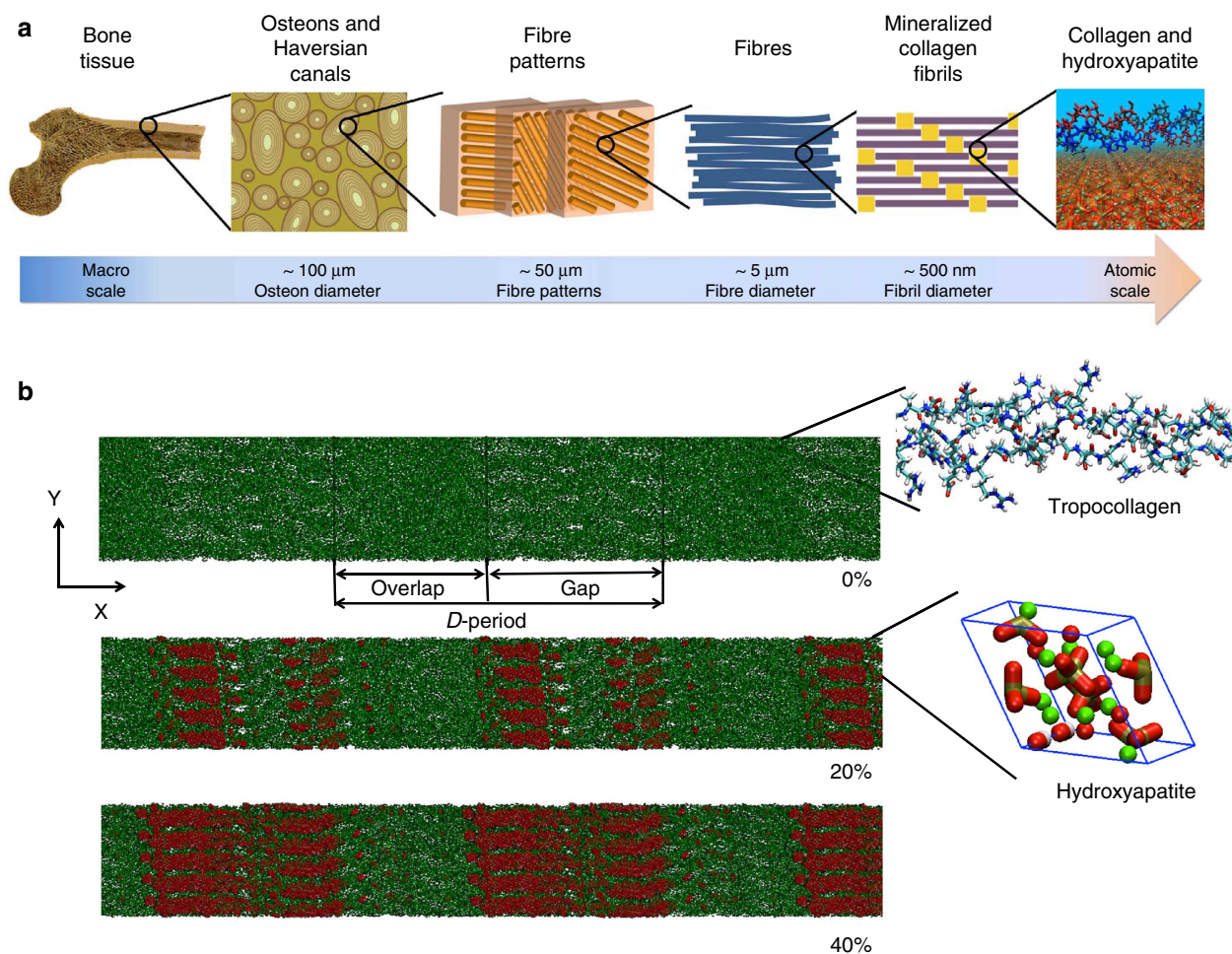


Figure 1 | Bone structure and model development. (a) Hierarchical structure of bone ranging from the macroscale skeleton to nanoscale collagen (green) and HAP (red). (b) Collagen microfibril model with 0% mineralization (inset shows the collagen triple-helix structure), 20% mineral content (inset shows a HAP unit cell) and 40% mineral content. The HAP crystals are arranged such that the c axis of crystal aligns with the fibril axis. Ca atoms plotted in green, OH groups plotted in red and white, and the tetrahedron structure visualizes the PO₄ group. The left three images in panel a taken from Launey et al.⁶⁵

interactions. The model also neglected the details of the shape or distribution of the mineral platelets, which is likely to have an important impact on the mechanical properties of the material.

In this paper we develop a three-dimensional, full-atomistic mineralized collagen microfibril model and perform tensile tests at various stress levels, to identify key deformation mechanisms. We find that as the mineral density increases, the tensile modulus increases successively, and is significantly larger than that of pure collagen fibrils. By comparing stress and strain fields associated with different mineral content and applied stress, we find that the mineral crystals carry about four times the stress compared with collagen, whereas the protein phase carries the bulk of deformation. These findings reveal the mechanism by which bone carries load at the nanoscale, where the district distribution of stress and strain between collagen and HAP enables a mechanism of great energy dissipation and resistance to fracture that overcomes the intrinsic limitations of the constituents and amplifies their superior properties.

Results

Mineralized microfibril model. We apply an *in silico* mineralization scheme based on a Monte Carlo approach, and identify molecular structures of nascent bone for different mineral densities, from 0% (pure collagen microfibril, see Fig. 1b for model details) to 40% (highly mineralized collagen fibril). As shown in Fig. 2a, the mineral is deposited predominantly in the gap region along the fibril axis, with sparse deposition in the overlap region. Figure 2b shows a detailed analysis of the distribution of mineral crystals for 20 and 40% mineral densities. We perform a direct comparison with experimental results that reported the distribution of mineral density as a function of the fibril axis²⁶, and plot the mineral distribution of 40% case normalized to its maximum value along with experimental results along the fibril axis (Fig. 2c). In good agreement with a rich set of experimental data^{1–6,26,27} in the mineralized microfibril models with varying densities (5, 10, 20, 40%, and so on), the mineral deposition occurs primarily in the gap region. This observation is also consistent with the experimental finding²⁶ that the mineral nucleation point is close to the carboxy terminus (in the first section of the gap region, immediately after the gap/overlap transition). As discussed by Nudelman *et al.*²⁶, the main reason is the high concentration of positive charge, which attract negatively charged peptides, in turn responsible for onset of mineralization. Our *in silico* mineralization process is not driven by electrostatic interactions (see Methods), but rather relies on a geometric argument, driven by the void space available within the virgin (non-mineralized) collagen fibril. This may suggest that in the *in vivo* mineralization process there could be concurrent mechanisms that lead to the nucleation in the C-terminal region. Along with the concentration of positive net charges, the C terminus region also features larger void spaces in the collagen packing, which makes this region the preferred site for mineral nucleation. We find that the 40% mineral-density case shows more mineral deposition in the gap region compared with experimental data²⁶. This could be due to the fact that in the experimental work, the mineral density profile is measured for collagen that is mineralized for 24 h. Our model shows that the size of the mineral platelets in the gap region is $\sim 15 \times 3 \times 1.6 \text{ nm}^3$ (for the case of 40% mineral density). This is in good agreement with experimental work that has shown that the size of mineral platelets is $15\text{--}55 \times 5\text{--}25 \times 2\text{--}3 \text{ nm}^3$ (refs 26–28). We note that the models are based on a periodic unit cell of a collagen microfibril with approximate dimensions of $67.8 \times 4 \times 2.7 \text{ nm}$ (see further discussion regarding structural aspects below). It is possible that the mineral phase can

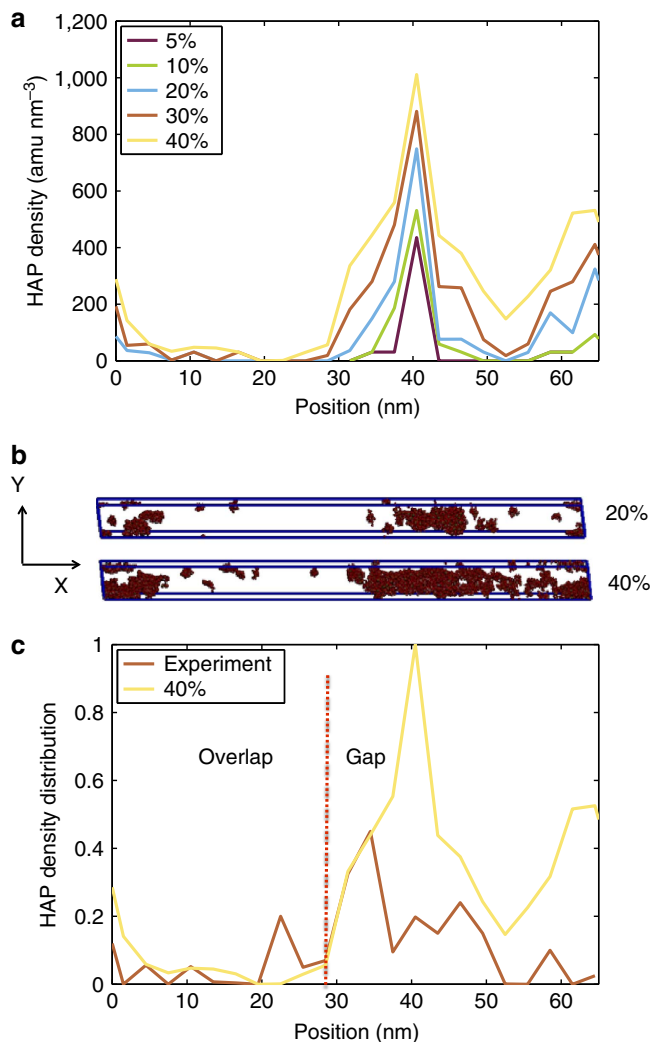


Figure 2 | Mineral distribution in the collagen microfibril at different mineralization stages. (a) Distribution of HAP along the collagen fibril axis. The data shows that the maximum amount of HAP is found in the gap region (between 30 and 50 nm). (b) Spatial distribution of HAP in the unit cell for 20 and 40% mineral density. (c) HAP density distribution along the fibril axis for the 40% case normalized (same data as depicted in panel a) compared with experimental data²⁶. The comparison confirms that maximum deposition is found in the gap region.

span several unit cells and, hence, forms larger size HAP platelets *in vivo*, explaining the larger range of values.

Mechanical testing. We carry out tensile tests on non-mineralized (0%), 20 and 40% mineral density samples (Fig. 3a). As observed from Fig. 3b, as the mineral content increases, the stress–strain behaviour of the mineralized collagen microfibril also changes compared with pure collagen fibrils, with the mineralized cases showing an increasingly higher modulus as higher mineral densities are reached. To quantify the variation of the modulus for different strain levels, we plot the modulus as a function of strain as shown in Fig. 3c. The 0% case has an initial modulus of 0.5 GPa at a load less than 20 MPa, and increases to 1.1 GPa as the stress increases to 100 MPa. For larger deformation, the modulus approaches 2 GPa. These moduli are well within the range of values reported for collagen fibrils under tensile loading using both experiment and simulation^{29,30}. For the 20% mineral-density case, the initial modulus is 1.3 GPa (stress

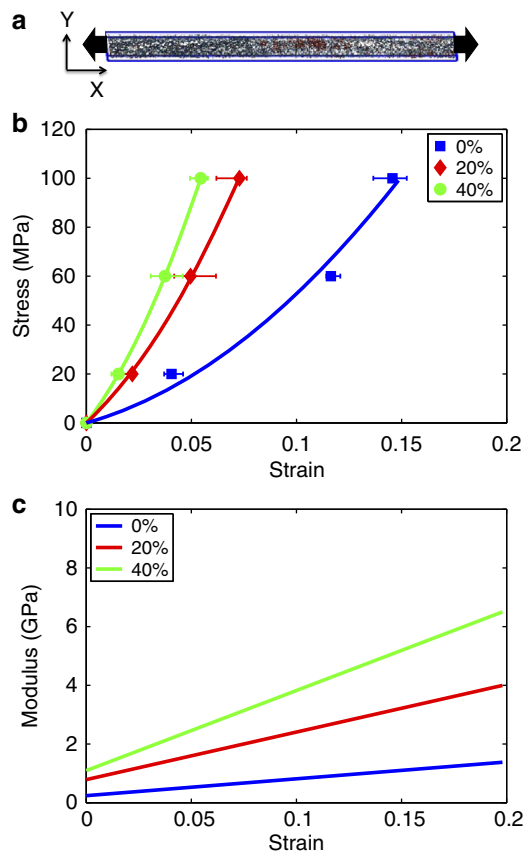


Figure 3 | Mechanical properties of collagen fibrils at different mineralization stages. (a) Fibril unit cell with mineral content used to perform tensile test by measuring stress versus strain. (b) Stress-strain plots for non-mineralized collagen fibril (0%), 20% mineral density and 40% mineral-density cases. (c) Modulus versus strain for 0, 20 and 40% mineral density showing an increase in modulus as the mineral content increases. The error bars in **b** are computed from the maximum and minimum values of the periodic box length along the x direction at equilibrium.

less than 20 MPa) and increases to 2.7 GPa at 100 MPa. This shows that even a relatively small mineral content severely alters the stress-strain behaviour of collagen microfibril model and increases its modulus by $\sim 150\%$. Similarly, the 40% mineral-density case has an initial modulus of 1.5 GPa, approaching 2.8 GPa. For stresses at 100 MPa, the 20 and 40% mineral-density cases have very similar tangent moduli. However, as shown in Fig. 3c, as the strain increases beyond 10%, the modulus for the 40% mineral-density case also increases, indicating that at higher strains the mineral content provides additional stiffness to the collagen-HAP composite. The moduli identified here for the cases with 20 and 40% mineral content is consistent with a recent experimental study³¹, which showed that mineralized collagen fibrils from antler had a modulus of 2.38 ± 0.37 GPa for strain less than 4%.

Nanoscale deformation mechanisms. To understand the deformation mechanism for mineralized and non-mineralized samples at different deformation states, we compute the deformation fields within the fibrils. We observe that as the loading increases, there is no significant movement or coalescence of the HAP crystals in the gap region when the loading increases from 20–100 MPa. However, for the 0% case, the collagen molecule undergoes significant deformation in the gap region as

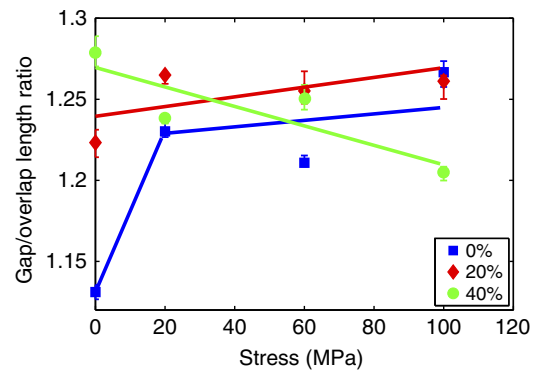


Figure 4 | Variation of the gap-to-overlap length ratio as the applied stress increases for different HAP contents. The deformation mechanism of non-mineralized collagen fibrils is molecular straightening in the crimped and loosely packed gap region (at small deformations), followed by molecular stretching (across the full *D*-period) at larger deformations. These mechanisms result in an initial increase in the gap/overlap ratio, which then remains constant, as is observed in the non-mineralized model reported here (where the gap/overlap ratio increases from 0–20 MPa stress). In contrast, in the mineralized cases the deformation mechanism is radically changed. Indeed, in the lower mineralized model (20% HAP) we do not observe any significant change in the gap/overlap ratio, suggesting that the *D*-period deforms rather uniformly, due to the stiffening effect of HAP mainly in the gap region. However, in the highly mineralized model (40% HAP), the trend is inverted, where the gap/overlap region decreases, suggesting that in this case the gap region is stiffer and that deformation takes place primarily in the overlap region. The error bars are obtained from the maximum and minimum values of the periodic box length along the x direction obtained after equilibration of each sample, which is utilized to compute the gap and overlap lengths.

the applied stress increases. We compute the deformation in the collagen microfibril for all three cases at applied stresses of 20, 60 and 100 MPa. As seen in Fig. 4, the gap-to-overlap ratio for 0% case increases with the applied stress, indicating that for pure collagen the gap region deforms significantly compared with the overlap region to accommodate the external load. This behaviour is consistent with earlier tensile tests on collagen microfibril³⁰. Clearly, the presence of HAP alters the deformation mechanism of the collagen fibril. For the 20% mineral-density case, the gap-to-overlap ratio is nearly constant for increases in applied stress, whereas for the 40% case the gap-to-overlap ratio decreases as the applied stress increases. This shows that a higher mineral content leads to more deformation in the overlap region compared with the gap region, where the interaction between HAP and collagen limits the deformation within collagen molecules. It has been previously suggested that the interaction between mineral and collagen is mainly due to electrostatic interactions and hydrogen bonding³². An analysis of the number of hydrogen bonds between the mineral and collagen in the gap region shows that the mineralized case has ~ 18 –20% more hydrogen bonds compared with the non-mineralized case, where the hydrogen bonding occurs solely between the chains within the collagen molecule. Another important mechanism of load transfer between collagen and HAP is due to salt bridges (electrostatic interactions between charged moieties). Although in the non-mineralized fibril this type of non-covalent interaction is minor, it becomes rather important in the mineralized samples. As shown in Fig. 5, the vast majority of salt bridges are formed within the mineral crystals; however, a non-negligible number of salt bridges are formed between mineral crystals and collagen, providing an effective load transfer mechanism between the mineral and

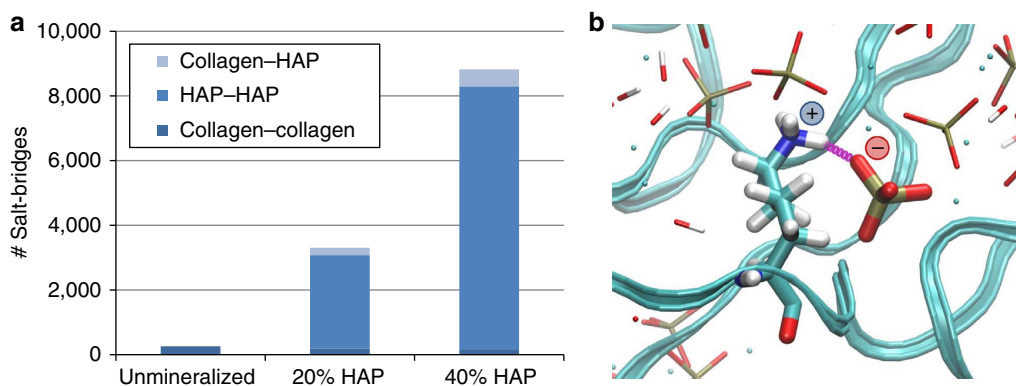


Figure 5 | Salt bridges in mineralized and non-mineralized collagen fibrils. (a) Number of salt bridges per unit cell. In the non-mineralized model, the number of salt bridges is ~ 260 , due to interactions between charged side chains of collagen: lysine (+), arginine (+), glutamic acid (–) and aspartic acid (–). In the mineralized models, there is a high number of mineral–mineral salt bridges, due to the fact that the moieties forming HAP are highly charged: Ca^{2+} , PO_4^{3-} and OH^- . Salt bridges are also found relevant between collagen and mineral phase (about 220 and 520 in 20% HAP and 40% HAP case, respectively), contributing to the increase in mechanical properties of mineralized fibrils. Panel **b** shows an example of salt bridge between a lysine (+) side chain and mineral PO_4^{3-} group.

organic phase that also enhances energy dissipation. This further explains our finding that the overlap region deforms more compared with gap region in the mineralized cases, a clear distinction from the mechanics of pure collagen fibrils.

Stress and strain distribution in non-mineralized and mineralized fibrils. To understand the distribution of stress inside the microfibril, we compute the stress distribution in the cross sectional y - z plane (Fig. 6a). The virial stresses³³ are computed for an applied stress of 100 MPa for 0%, 20% and 40% mineral-density cases, respectively. To visualize and quantify the stresses in the unit cell, we compute the principal stresses for a region with a finite thickness of 15 Å in the x direction. For the 0% case we choose the overlap region, and for the 20 and 40% mineral-density cases we chose the gap region for principal stress computation. As observed from Fig. 6a, the 0% case has a nearly uniform stress distribution with maximum stresses reaching ~ 15 MPa, indicating that the collagen backbone gets stretched and the three chains take the load. The mineralized cases show higher stress in HAP compared with collagen, with maximum stress reaching 50 MPa, hence suggesting that the load is predominantly carried by the mineral phase. To validate this finding, we plot the average stress in collagen and the mineral phase for 20 and 40% mineral densities. Figure 6b shows that the HAP phase takes approximately four times the stress compared with collagen. This leads to the conclusion that as the mineral content increases, there is a stronger interaction between the mineral and the collagen, and that the applied load is distributed among collagen and mineral phases in a particular pattern.

To quantify the strain distribution in the collagen and HAP phase, we compute the end-to-end distance for collagen molecule at 0 and 100 MPa. From the computed difference in end-to-end length for 0 and 100 MPa applied stresses, we find that the collagen phase with mineral density of 20% takes 7.3% strain, whereas for 40% mineral density the strain is 6.3%. For the HAP phase, we estimate the strain from the bulk modulus of HAP (100 GPa computed from our model, and is in good agreement with previous studies³⁴) along the x axis at an applied stress of 100 MPa. The value of strain in the HAP phase is 0.06%, which is two orders of magnitude lower than the strain in the collagen phase. These findings and our observation that the strain in collagen is lower than the total strain is in very good agreement

with earlier studies^{4,35}, and suggests that in the mineralized collagen microfibril the collagen deforms significantly more than the HAP crystals. We also compute the stress in mineral platelets from the strain values of mineral as reported in Gupta *et al.*⁴ and using a modulus of 100 GPa. The stress in the mineral at 100 MPa applied stress is ~ 110 MPa. We note that the stress in the mineral is higher (by approximately two times) than the value we obtained from our model. This could be because of the fact that our model does not include extrafibrillar mineral content, and that the extrafibrillar mineral content could have an important role in stress transfer between fibrils by shear deformation as suggested earlier⁴.

Mineral crystals carry more stress, whereas the collagen protein carries more deformation. This distribution of stress and strain between collagen and HAP at the nanoscale enables a mechanism of energy dissipation and, as such, resistance to fracture in bone. As observed in a recent atomistic study²³ that focused on the interface between collagen and HAP, a collagen molecule at high stress levels gets stretched and starts to uncoil, and eventually slides on the HAP surface. Our mineralized microfibril model, the deformation process at low stress levels, indicates the onset of such a deformation mechanism, where the overlap region deforms more compared with the gap region.

Discussion

Although available models of mineralized fibrils reflect a range of theoretical and analytical models (even if very complex), our model for the first time accounts for the full biochemistry of mineralized fibrils, as it is an all-atom molecular model. The model can easily be adapted to other collagen sequences, geometries or bone types, and is hence anticipated to have broad impact for future modelling and experimental work. As a consequence of the fundamental approach, our model is not only able to correctly predict the gross mechanical properties of mineralized fibrils, but it also allows obtaining fundamental insights on the nanoscale deformation mechanisms and on the load transfer between collagen and mineral. For example, the parameters derived from our model can be incorporated into existing analytical models^{13,36,37} and can provide parameter estimates from a fundamental perspective. We specifically compare two analytical approaches reported in (refs 36–38) with the simulation and experimental results³¹ (details of the analytical models see Methods). As observed from Fig. 7, Gao's

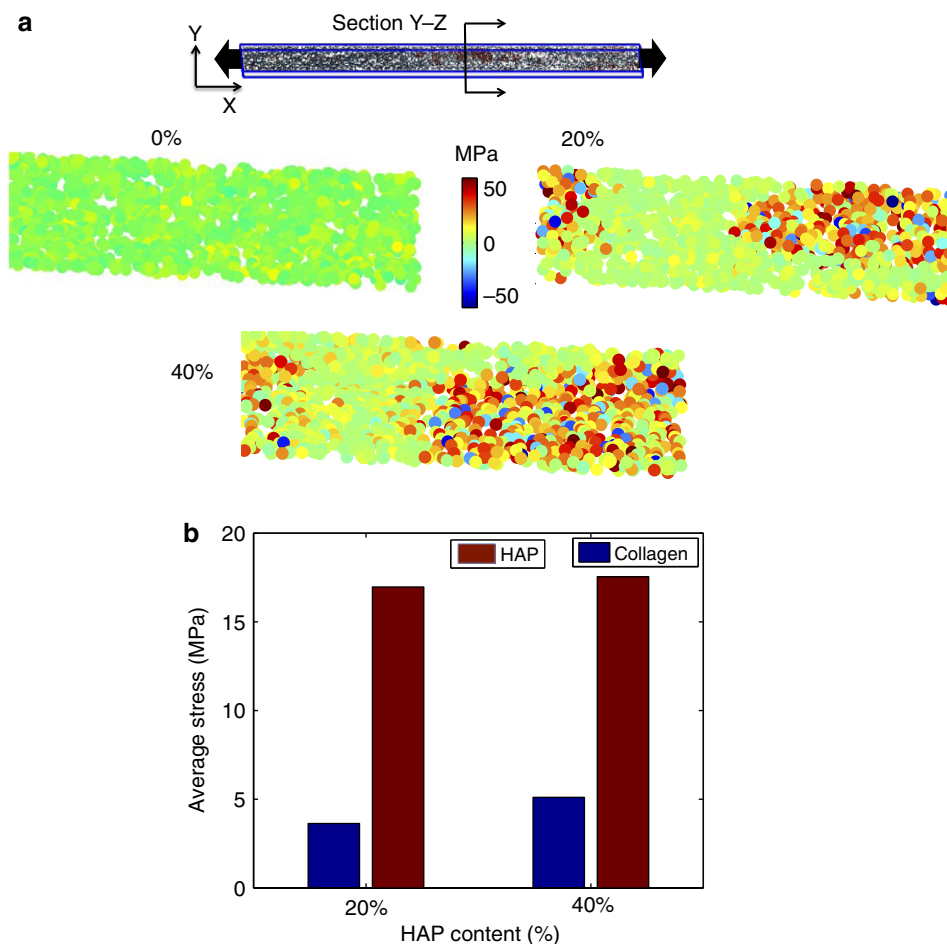


Figure 6 | Analysis of stress fields for different mineral contents. (a) View of the cross-section of the y-z plane of the unit cell used to perform the stress analysis. The principal stress contours for an applied stress of 100 MPa in collagen microfibril show a nearly uniform stress distribution, whereas the data for 20 and 40% mineral-density cases clearly reveals significantly higher stress regions in the HAP mineral. (b) Quantification of the overall average stress in the collagen and mineral phases at 100 MPa applied stress, showing that the mineral phase features about four times the stress level compared with collagen.

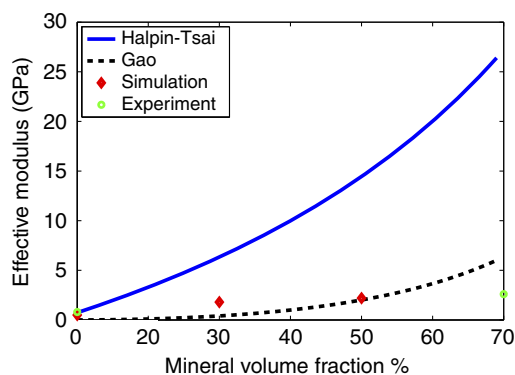


Figure 7 | Variation of effective modulus with respect to mineral volume fraction comparing simulation, experiment and analytical models.

Comparison of analytical models by Halpin-Tsai^{36,38} and Gao *et al.*³⁷ with our simulation data and experimental results³¹. The analytical model by Halpin-Tsai (equations (1) and (2)) predicts a higher modulus as the mineral volume fraction increases compared with Gao's model, simulation and experimental modulus. The Gao model (equation (3)) agrees better overall, but predicts a lower modulus for very low mineral content and deviates from the atomistic and experimental predictions for higher mineral content.

model³⁷ predicts a slightly lower modulus for low mineral volume fraction and increases as the mineral volume fraction increases, but is consistent with atomistic and experimental values for high mineral volume fraction. The Halpin-Tsai bone model^{36,38} predicts a much higher modulus compared with Gao's model, simulation results and experimental data, as the mineral volume fraction increases. The difference between the analytical models is likely due to the fact that Gao's model was developed from the experimental observation of the bone nanostructure, which explains the overall good agreement. Moreover, in Gao's model the effective stiffness depends on the shear modulus G_p of the collagen, which is several orders of magnitude lower than the modulus of the mineral. Hence, at low mineral volume fractions the effective modulus is likely dominated by the shear modulus and the aspect ratio of the mineral ($G_p \rho^2$). The difference between analytical models and simulations could be due to the assumption in the analytical model that minerals are rectangular blocks, and that the mineral size and shape doesn't change in the gap and overlap regions. Therefore, one possible insight derived from this comparison is that the variation of mineral size and shape in the gap and overlap region controls the effective modulus and deformation mechanisms at the nanoscale, and must be taken into consideration.

Our model predicts the characteristic elongated shape of mineral platelets with an ultra-small thickness on the order of a few nanometers (approximate crystal dimensions $\sim 15 \times 3 \times 1.6 \text{ nm}^3$). The geometric confinement to very thin nanometer crystals has been suggested to have a critical role in achieving flow tolerance³⁷, a phenomenon that has been confirmed in full-atomistic simulation³⁹. Mineral crystals at that size are no longer brittle (as they are at the macro scale, for example, classroom chalk), but instead show a highly ductile behaviour³⁹. As the mineral content increases from 20–40%, the modulus increases continuously, confirming that mineral deposition leads to significant stiffening during bone formation. The detailed understanding of the mechanics of this process could be important in identifying the cellular response to changes in the mechanical microenvironment^{26,40,41}, as well as for models of bone remodelling and tissue engineering^{1,2,9,42,43}. The load transfer mechanism between the organic phase (collagen) and the inorganic phase (HAP) is due to electrostatic interactions, namely hydrogen bonds and salt bridges. These interactions can explain the enhanced capacity to dissipate energy as it enables a stick–slip deformation process activated at large deformation. Altogether, the mineral crystals carry more stress, whereas the collagen protein carries more deformation. This distribution of stress and strain is critical, as it takes advantage of the great stiffness of minerals and the energy dissipating capacity of collagen molecules through uncoiling of their triple helical structure, similar to sacrificial mechanisms observed at larger scales⁴⁴. This, together with the confinement of minerals to very thin nanometer dimensions, suggests that the nanocomposite in bone is a means to overcome the intrinsic limitations of each of the constituents, and to form a composite that amplifies the superior properties of the two.

Our model opens a new possibility to study bone nano-mechanics; for example, investigating the effect of mineral shape, size and orientation with chemical detail. In future work, the model developed here can also be applied to study brittle bone disease and other bone disorders, setting the stage for many fundamental investigations. Other future efforts could focus on further structure refinement of the model and additional experimental validation, in particular considering the distribution of mineral at larger-length scales.

Methods

Model overview. The goal is to develop a full-atomistic model that enables us to perform a systematic study of bone nanomechanics from a fundamental, molecular point of view. This goes beyond earlier theoretical, computational and analytical models (references and discussion see main text) that do not include the full biochemical details, and allows us to ask questions such as ‘what is the deformation mechanism in bone fibrils?’ or ‘what is the load transfer mechanism between collagen and mineral platelets?’. The geometry and composition of the model are summarized in Fig. 1b, indicating varied levels of mineral content. The 0% case corresponds to a non-mineralized collagen microfibril and also clearly shows the gap and overlap region (Fig. 1b) that emerges from the geometrical arrangement of collagen protein molecules. The *D*-period corresponds to the periodicity typically observed in collagen fibrils. The 20 and 40% mineral-density cases correspond to the two different mineral concentrations in the collagen microfibril. A recent study³⁰ conducted of a pure collagen fibril has shown good agreement with experimental results. This prior work forms the basis for the model of bone, accomplished here by incorporating minerals in collagen in increasing densities (as it occurs naturally during bone formation), whereas accounting for the complexity of the chemical interactions^{26,45–47} that have not yet been incorporated in earlier models.

Collagen protein force field parameterization. Collagen is the sole protein that features hydroxyproline (HYP), a non-standard amino acid, resulting from the post-translational hydroxylation of proline. As it is rarely found, HYP is not parameterized in common biomolecular force fields, such as CHARMM⁴⁸. However, a set for HYP has been developed⁴⁹ based on quantum mechanical models and have been subsequently used to derive the atomistic parameters that best match the quantum-mechanics calculation, with particular focus on the

correct modelling of the pucker of the HYP ring. These parameters have been then successfully incorporated into an extended CHARMM force field as used for collagen modelling in a series of previous works^{30,50,51}. This model is also used here.

Crystal geometry and HAP force field parameterization. We generated the hexagonal HAP crystal unit cell by using Material Studio 4.4 (Accelrys, Inc.), which features the following lattice parameters: $a = 9.4214 \text{ \AA}$, $b = 9.4214 \text{ \AA}$, $c = 6.8814 \text{ \AA}$, $\alpha = 90^\circ$, $\beta = 90^\circ$ and $\gamma = 120^\circ$. On the basis of this unit cell (with 44 atoms per unit cell), HAP crystals of varying size are generated for the purpose of this study, using the *in silico* mineralization method described below. Force fields for biomaterial simulations like CHARMM⁴⁸ do not include parameters for mineral crystal, such as HAP. Therefore, to model protein–HAP composites, we extend the CHARMM force field and use bond, angle and dihedral parameters following those reported earlier⁵², which are based on both quantum mechanical calculations and empirical data. For non-bonded parameters, we adopt a Born–Mayer–Huggins model. For non-bonded terms, we use data from Bhowmik *et al.*⁵³ in which the authors fitted the Born–Mayer–Huggins potential⁵² with a simpler Lennard–Jones potential.

Mineralized collagen microfibril model: *in silico* mineralization. The collagen microfibril model used here is based on Protein Data Bank entry 3HR2 that was used as a basis for the non-mineralized collagen fibril model reported in ref. 30. For further information, we refer the reader to a previous paper with the details on the development of the collagen fibril atomistic model³⁰ and to the work that describes the details of the X-ray crystallography⁵⁴. The mineralized models are built starting from the non-mineralized model by filling the model’s periodic box of HAP unit cells. Then, the HAP unit cells that have at least one atom overlapping with the atoms of collagen are removed. In this way, the HAP is left only in void space of the collagen fibril box. The overlapping condition is controlled by a chosen cutoff distance between HAP atoms and collagen atoms. By selecting the appropriate cutoff distance, it is possible to add more or less HAP unit cells and, thus, reach varied degrees of mineralization. This procedure is implemented through a tcl script used in the Visual Molecular Dynamics programme⁵⁵. The choice of physiologically relevant amounts of HAP is chosen based on the literature^{2,56}, which show that the content of the mineral phase is 60–70% w/w of bone tissue. In addition to the crystallites associated with the collagen fibrils (intrafibrillar mineralization), a significant amount of mineral is believed to be located in the spaces between the fibrils (extrafibrillar mineralization). It has been reported that the extrafibrillar mineral fraction can account to as much as 75% of the total mineral in bone tissues^{57–59}. Therefore, in our models, which account only for interfibrillar mineralization, we consider degrees of mineralization of up to 40%, which allows us to study moderately to highly mineralized fibrils. The orientation and surface of HAP crystals also has a significant effect in controlling the collagen–mineral interactions. Recent studies using density functional theory shows that the mineral crystal surface (that is, either a OH- or a Ca-terminated surface) has a significant role in controlling the interaction between collagen and HAP⁶⁰. In our model, the mineral crystals are oriented such that orientation of the OH groups of the crystal is parallel to the collagen fibril axis as shown in Fig. 1b. This orientation of crystals and the growth of the crystals along the fibril axis typically observed in experiments⁵⁶ are, hence, consistent with our mineralized collagen microfibril model. The mineral distribution inside the unit cell and its densities are shown in Fig. 2a, b. To enable a direct comparison with experimental results for mineral distribution, we utilize the density distribution for non-mineralized and mineralized collagen as reported in Nudelman *et al.*²⁶, and plot the difference of the two data sets in comparison with our 40% mineral-density case (Fig. 2c). It is important to note that the *in vivo* mineralization process is a very complex phenomenon, in which immature amorphous HAP clusters nucleate close to the C-terminal end (which is at the gap-to-overlap transition region), and then grow by further mineral deposition. Furthermore, the process is believed to be assisted by acidic non-collagenous proteins. This process is too complex to be reliably replicated with direct atomistic simulations. Hence, our approach is to mimic the mineralization process by filling the void space within the collagen unit cell, in the process described above. Future works could be devoted to improve the *in silico* model of the mineralization process, to mimic more closely the *in vivo* mature mineralization state.

Fibril equilibration. Molecular dynamics simulations are performed using the LAMMPS code⁶¹ and the modified CHARMM force field described above. The constructed collagen–HAP model is first geometrically optimized through energy minimization, and then an NVT equilibration is performed for 2 ns. The unit cell that comprises collagen and HAP has triclinic symmetry as described in earlier work³⁴. Rigid bonds are used to constrain covalent bond lengths, thus allowing for an integration time step of 2 fs. Non-bonding interactions are computed using a switching function between 0.8 and 1.0 nm for van der Waals interactions, whereas the Ewald summation method⁶² is applied to describe electrostatic interactions. The system temperature is maintained at 300 K (room temperature). We confirmed that the root mean square deviation of the mineralized collagen is stable, and that no major changes occur in the structure towards the end of equilibration.

In silico mechanical testing. To assess the mechanical properties of mineralized collagen fibrils, we perform stress-controlled ($NP_{ij}T$) molecular dynamics simulations with increasing tensile stress applied along the x axis of the unit cell as depicted in Fig. 3a. The unit cell is under constant atmospheric pressure along other two axes (y and z). We use an $NP_{ij}T$ ensemble⁶³ for loading the samples with different stress states ($\sigma = -P_{ij}$) ranging from: (i) atmospheric pressure, (ii) 20 MPa, (iii) 60 MPa and (iv) 100 MPa. We observe that samples reached equilibration under applied load at ~ 6 ns. The strain is computed as $\varepsilon = (L - L_0)/L_0$, where L_0 is the equilibrium length identified at atmospheric pressure. To ensure that equilibrium is achieved, we monitor the pressure at equilibrium, root mean square deviation, and confirm that the size of the simulation cell reaches a steady-state value. Using the fibril strain ε associated with each applied stress σ , we obtain the stress-strain behaviour for each case by plotting σ over ε . We use a second-order polynomial function to fit the stress-strain data, which includes all positive coefficients. The general form of the equation is $\sigma = a_1\varepsilon^2 + a_2\varepsilon$. For both non-mineralized and mineralized data sets, the coefficients a_1 and a_2 are positive so that the fitting procedure is consistent. The modulus is computed from the first derivative of a polynomial function that is fitted to the stress-strain data. The polynomial functions that are used to fit the stress-strain data are as follows: (a) for the 0% case, $2874.9x^2 + 240.61x$; (b) for the 20% case, $8101.8x^2 + 787.89x$; and (c) for the 40% case, $13651x^2 + 1094.2x$ (with appropriate dimensions to express stress in MPa). The computational time requirement for equilibration is 0.2 ns per week using 24 processors for the 40% mineral-density case.

Visualization. We use Visual Molecular Dynamics⁵⁵ to visualize the snapshots of simulation and compute hydrogen bonds. We count the hydrogen bonds within a cutoff distance of 3.5 Å and an angle range of 30°. MATLAB (MathWorks, Inc.) is used to plot the stress distribution inside the collagen microfibril model.

Strain analysis. We find the distance between the centre of mass of glycine residues in each chain of the collagen triple helix, and then utilize the distance between the centre of mass to compute the total deformation in collagen microfibril. This approach of computing the strain in a collagen molecule has been discussed in detail in earlier work⁶⁴, and the readers are referred to this article for further information. Once the deformation is obtained for the whole microfibril, we compute the deformation of the gap and overlap region.

Theoretical models. We compare the effective modulus predicted by atomistic simulations with analytical models by Halpin-Tsai^{36,38} and Gao *et al.*³⁷, and also with the experimental values reported in Hang and Barber³¹. According to the Halpin-Tsai model, the longitudinal modulus of a unidirectional plane, parallel platelet-reinforced composite is given by

$$\hat{E} = E_m \frac{1 + AB\Phi}{1 - B\Phi} \quad (1)$$

where E_m is the matrix modulus (here we use 0.5 GPa as the value obtained from our non-mineralized sample) and Φ is the mineral volume fraction. The constants A and B are given by

$$A = 2\rho, \text{ and } B = \frac{\left(\frac{E_p}{E_m} - 1\right)}{\left(\frac{E_p}{E_m} + A\right)} \quad (2)$$

where ρ is the aspect ratio of the mineral (for biological materials, such as bone $\rho \sim 30$) and E_p is the modulus of the mineral platelet (100 GPa). According to Gao *et al.*³⁷, the effective modulus for a nanocomposite is given by

$$\frac{1}{\hat{E}} = \frac{4(1 - \Phi)}{G_p \rho^2} + \frac{1}{E_{mg} \Phi} \quad (3)$$

where Φ is the mineral volume fraction, E_{mg} is the elastic modulus of mineral (100 GPa), ρ is the aspect ratio of the mineral (for bone $\rho \sim 30$) and $G_p = 0.03$ GPa is the shear modulus of collagen. The comparison of the analytical models, simulation and experiments are shown in Fig. 7.

Force field files, scripts and atomic structure files. The force-field files for LAMMPS, structure files in PDB format and all scripts used in this study are available from the corresponding author upon request.

References

1. Fratzl, P. (ed.). *Collagen: Structure and Mechanics* (Springer, 2008).
2. Fratzl, P., Gupta, H. S., Paschalis, E. P. & Roschger, P. Structure and mechanical quality of the collagen-mineral nano-composite in bone. *J. Mater. Chem.* **14**, 2115–2123 (2004).
3. Fratzl, P. & Weinkamer, R. Nature's hierarchical materials. *Prog. Mater. Sci.* **52**, 1263–1334 (2007).
4. Gupta, H. S. *et al.* Cooperative deformation of mineral and collagen in bone at the nanoscale. *Proc. Natl Acad. Sci. USA* **103**, 17741–17746 (2006).
5. Jager, I. & Fratzl, P. Mineralized collagen fibrils: a mechanical model with a staggered arrangement of mineral particles. *Biophys. J.* **79**, 1737–1746 (2000).
6. Weiner, S. & Wagner, H. D. The material bone: structure mechanical function relations. *Annu. Rev. Mater. Sci.* **28**, 271–298 (1998).
7. Fratzl, P. Bone fracture - when the cracks begin to show. *Nat. Mater.* **7**, 610–612 (2008).
8. Koester, K. J., Ager, J. W. & Ritchie, R. O. The true toughness of human cortical bone measured with realistically short cracks. *Nat. Mater.* **7**, 672–677 (2008).
9. Taylor, D., Hazenberg, J. G. & Lee, T. C. Living with cracks: damage and repair in human bone. *Nat. Mater.* **6**, 263–268 (2007).
10. Nalla, R. K., Kinney, J. H. & Ritchie, R. O. Mechanistic fracture criteria for the failure of human cortical bone. *Nat. Mater.* **2**, 164–168 (2003).
11. Taylor, D. Fracture mechanics - how does bone break? *Nat. Mater.* **2**, 133–134 (2003).
12. Tai, K., Dao, M., Suresh, S., Palazoglu, A. & Ortiz, C. Nanoscale heterogeneity promotes energy dissipation in bone. *Nat. Mater.* **6**, 454–462 (2007).
13. Liu, G., Ji, B. H., Hwang, K. C. & Khoo, B. C. Analytical solutions of the displacement and stress fields of the nanocomposite structure of biological materials. *Comp. Sci. Technol.* **71**, 1190–1195 (2011).
14. Kotha, S. P. *A Micromechanical Model to Explain the Mechanical Properties of Bovine Cortical Bone in Tension: in vitro Fluoride Ion Effects* (Rutgers University and Robert Wood Johnson Medical School, 2000).
15. Zuo, S. C. & Wei, Y. G. Effective elastic modulus of bone-like hierarchical materials. *Acta Mech. Solida Sin.* **20**, 198–205 (2007).
16. Bar-On, B. & Wagner, H. D. Mechanical model for staggered bio-structure. *J. Mech. Phys. Solids* **59**, 1685–1701 (2011).
17. Zhang, Z. Q., Liu, B., Huang, Y., Hwang, K. C. & Gao, H. Mechanical properties of unidirectional nanocomposites with non-uniformly or randomly staggered platelet distribution. *J. Mech. Phys. Solids* **58**, 1646–1660 (2010).
18. Zhang, D. J., Chippada, U. & Jordan, K. Effect of the structural water on the mechanical properties of collagen-like microfibrils: A molecular dynamics study. *Ann. Biomed. Eng.* **35**, 1216–1230 (2007).
19. Duchstein, P. & Zahn, D. Atomistic modeling of apatite-collagen composites from molecular dynamics simulations extended to hyperspace. *J. Mol. Model.* **17**, 73–79 (2011).
20. Zahn, D., Hochrein, O., Kawska, A., Brickmann, J. & Knip, R. Towards an atomistic understanding of apatite-collagen biomaterials: linking molecular simulation studies of complex-, crystal- and composite-formation to experimental findings. *J. Mater. Sci.* **42**, 8966–8973 (2007).
21. Bhowmik, R., Katti, K. S. & Katti, D. R. Mechanics of molecular collagen is influenced by hydroxyapatite in natural bone. *J. Mater. Sci.* **42**, 8795–8803 (2007).
22. Bhowmik, R., Katti, K. S. & Katti, D. R. Mechanisms of load-deformation behavior of molecular collagen in hydroxyapatite-tropocollagen molecular system: Steered Molecular Dynamics Study. *J. Eng. Mech.* **135**, 413–421 (2009).
23. Zhao, Q., Alfonso, G., Nair, A. K., Inbar, H. & Buehler, a. M. J. Thickness of hydroxyapatite nanocrystal controls mechanical properties of the collagen - hydroxyapatite interface. *Langmuir* **28**, 1982–1992 (2012).
24. Boskey, A. Bone mineral crystal size. *Osteop. Int.* **14**, S16–S20 (2003).
25. Buehler, M. J. Molecular nanomechanics of nascent bone: fibrillar toughening by mineralization. *Nanotechnology* **18**, 295102 (2007).
26. Nudelman, F. *et al.* The role of collagen in bone apatite formation in the presence of hydroxyapatite nucleation inhibitors. *Nat. Mater.* **9**, 1004–1009 (2010).
27. Alexander, B. *et al.* The nanometre-scale physiology of bone: steric modelling and scanning transmission electron microscopy of collagen-mineral structure. *J. R. Soc. Interf.* **9**, 1774–1786 (2012).
28. Fratzl, P., Fratzl-Zelman, N., Klaushofer, K., Vogl, G. & Kristian, K. Nucleation and growth of mineral crystals in bone studied by small-angle X-ray scattering. *Calc. Tissue Int.* **48**, 407–413 (1991).
29. Van Der Rijt, J. A. J., Van Der Werf, K. O., Bennink, M. L., Dijkstra, P. J. & Feijen, J. Micromechanical testing of individual collagen fibrils. *Macromol. Biosci.* **6**, 699–702 (2006).
30. Gautieri, A., Vesentini, S., Redaelli, A. & Buehler, M. J. Hierarchical structure and nanomechanics of collagen microfibrils from the atomistic scale up. *Nano Lett.* **11**, 757–766 (2011).
31. Hang, F. & Barber, A. H. Nano-mechanical properties of individual mineralized collagen fibrils from bone tissue. *J. R. Soc. Interf.* **8**, 500–505 (2011).
32. Kikuchi, M., Itoh, S., Ichinose, S., Shinomiya, K. & Tanaka, J. Self-organization mechanism in a bone-like hydroxyapatite/collagen nanocomposite synthesized *in vitro* and its biological reaction *in vivo*. *Biomaterials* **22**, 1705–1711 (2001).
33. Zimmerman, J. A. *et al.* Calculation of stress in atomistic simulation. *Model. Simul. Mater. Sci. Eng.* **12**, S319–S332 (2004).
34. Menéndez-Prupina, E. *et al.* Computer simulation of elastic constants of hydroxyapatite and fluorapatite. *J. Mech. Behav. Biomed. Mater.* **4**, 1011–1020 (2011).
35. Gupta, H. S. *et al.* Synchrotron diffraction study of deformation mechanisms in mineralized tendon. *Phys. Rev. Lett.* **93**, 158101 (2004).

36. Haplin, J. C. & Kardos, J. L. The Haplin-Tsai equations: a review. *Pol. Eng. Sci.* **16**, 344–352 (1976).
37. Gao, H., Ji, B., Jager, I. L., Arzt, E. & Fratzl, P. Materials become insensitive to flaws at nanoscale: Lessons from nature. *Proc. Natl Acad. Sci. USA* **100**, 5597–5600 (2003).
38. Akiva, U., Wagner, H. D. & Weiner, S. Modelling the three-dimensional elastic constants of parallel-fibred and lamellar bone. *J. Mater. Sci.* **33**, 1497–1509 (1998).
39. Libonati, F., Nair, A. K., Vergani, L. & Buehler, M. J. Fracture mechanics of hydroxyapatite single crystals under geometric confinement. *J. Mech. Behav. Biomed. Mater* **20**, 184–191 (2013).
40. Engler, A. J., Sen, S., Sweeney, H. L. & Discher, D. E. Matrix elasticity directs stem cell lineage specification. *Cell* **126**, 677–689 (2006).
41. Huebsch, N. & Mooney, D. J. Inspiration and application in the evolution of biomaterials. *Nature* **462**, 426–432 (2009).
42. Meinel, L. *et al.* Silk implants for the healing of critical size bone defects. *Bone* **37**, 688–698 (2005).
43. Alsberg, E. *et al.* Regulating bone formation via controlled scaffold degradation. *J. Dent. Res.* **82**, 903–908 (2003).
44. Fantner, G. E. *et al.* Sacrificial bonds and hidden length dissipate energy as mineralized fibrils separate during bone fracture. *Nat. Mater.* **4**, 612–616 (2005).
45. Xie, B. Q. & Nancollas, G. H. How to control the size and morphology of apatite nanocrystals in bone. *Proc. Natl Acad. Sci. USA* **107**, 22369–22370 (2010).
46. Chung, W. J., Kwon, K. Y., Song, J. & Lee, S. W. Evolutionary screening of collagen-like peptides that nucleate hydroxyapatite crystals. *Langmuir* **27**, 7620–7628 (2011).
47. Almora-Barrios, N. & De Leeuw, N. H. Molecular dynamics simulation of the early stages of nucleation of hydroxyapatite at a collagen template. *Cryst. Growth Design* **12**, 756–763 (2012).
48. Brooks, B. R. *et al.* Charmm - a program for macromolecular energy, minimization, and dynamics calculations. *J. Comput. Chem.* **4**, 187–217 (1983).
49. Park, S., Radmer, R. J., Klein, T. E. & Pande, V. S. A new set of molecular mechanics parameters for hydroxyproline and its use in molecular dynamics simulations of collagen-like peptides. *J. Comput. Chem.* **26**, 1612–1616 (2005).
50. Gautieri, A., Buehler, M. J. & Redaelli, A. Deformation rate controls elasticity and unfolding pathway of single tropocollagen molecules. *J. Mech. Behav. Biomed. Mater.* **2**, 130–137 (2009).
51. Gautieri, A., Uzel, S., Vesentini, S., Redaelli, A. & Buehler, M. J. Molecular and mesoscale mechanisms of osteogenesis imperfecta disease in collagen fibrils. *Biophys. J.* **97**, 857–865 (2009).
52. Hauptmann, S., Dufner, H., Brickmann, J., Kast, S. M. & Berry, R. S. Potential energy function for apatites. *Phys. Chem. Chem. Phys.* **5**, 635–639 (2003).
53. Bhowmik, R., Katti, K. S. & Katti, D. Molecular dynamics simulation of hydroxyapatite-polyacrylic acid interfaces. *Polymer* **48**, 664–674 (2007).
54. Orgel, J. P. R. O., Irving, T. C., Miller, A. & Wess, T. J. Microfibrillar structure of type I collagen in situ. *Proc. Natl Acad. Sci. USA* **103**, 9001–9005 (2006).
55. Humphrey, W., Dalke, A. & Schulten, K. VMD: Visual molecular dynamics. *J. Mol. Graph.* **14**, 33–38 (1996).
56. Beniash, E. Biomaterials—hierarchical nanocomposites: the example of bone. *Wiley Interdisc. Rev. Nanomed. Nanobiotechnol.* **3**, 47–69 (2011).
57. Lees, S., Prostack, K. S., Ingle, V. K. & Kjoller, K. The loci of mineral in turkey leg tendon as seen by atomic-force microscope and electron-microscopy. *Calc. Tissue Int.* **55**, 180–189 (1994).
58. Bonar, L. C., Lees, S. & Mook, H. A. Neutron-diffraction studies of collagen in fully mineralized bone. *J. Mol. Biol.* **181**, 265–270 (1985).
59. Kinney, J. H. *et al.* Intrafibrillar mineral may be absent in dentinogenesis imperfecta type II (DI-II). *J. Dent. Res.* **80**, 1555–1559 (2001).
60. Almora-Barrios, N. & de Leeuw, N. H. A density functional theory study of the interaction of collagen peptides with hydroxyapatite surfaces. *Langmuir* **26**, 14535–14542 (2010).
61. Humphrey, J. D., Wells, P. B., Thomsen, S., Jones, M. A. & Baek, S. Histological evidence for the role of mechanical stress in modulating thermal denaturation of collagen. *Biomech. Model. Mechanobiol.* **4**, 201–210 (2005).
62. in't Veld, P. J., Ismail, A. E. & Grest, G. S. Application of Ewald summations to long-range dispersion forces. *J. Chem. Phys.* **127** (2007).
63. Plimpton, S. Fast parallel algorithms for short-range molecular-dynamics. *J. Comput. Phys.* **117**, 1–19 (1995).
64. Chang, S. W., Shefelbine, S. J. & Buehler, M. J. Structural and mechanical differences between collagen homo- and heterotrimers: relevance for the molecular origin of brittle bone disease. *Biophys. J.* **102**, 640–648 (2012).
65. Launey, M. E., Buehler, M. J. & Ritchie, R. O. On the mechanistic origins of toughness in bone. *Annu. Rev. Mater. Sci.* **40**, 4175–4188 (2010).

Acknowledgements

We acknowledge support from the Office of Naval Research (N000141010562) and the Army Research Office (W991NF-09-1-0541 and W911NF-10-1-0127), with additional support from the National Science Foundation (CMMI-0642545). Support was also provided by the MIT-Italy Program ('Progetto Rocca') and Politecnico di Milano (Grant '5 per mille junior 2009'). High-performance computing resources were provided by the Regione Lombardia and CILEA Consortium through the LISA Initiative, and by CINECA under the ISCRA initiative, as well as the National Science Foundation XSEDE programme (MSS090007).

Author contributions

M.J.B., A.G. and A.K.N. designed the research. A.G., A.K.N. and S.-W.C. implemented the model and analysis tools, carried out the simulations and collected the data. M.J.B., A.K.N., A.G. and S.-W.C. analysed the data and wrote the paper.

Additional information

Competing financial interests: The authors declare no competing financial interests.

Reprints and permission information is available online at <http://npg.nature.com/reprintsandpermissions/>

How to cite this article: Nair, A. K. *et al.* Molecular mechanics of mineralized collagen fibrils in bone. *Nat. Commun.* **4**:1724 doi: 10.1038/ncomms2720 (2013).



This work is licensed under a Creative Commons Attribution-NonCommercial-ShareAlike 3.0 Unported License. To view a copy of this license, visit <http://creativecommons.org/licenses/by-nc-sa/3.0/>